Supplementary Information

Microdroplets as ambient 'hydrothermal' reactors

Anand Narayanan,[a] Anubhav Mahapatra,[a] Sonali Seth,[a] Sinchan Mukhopadhyay,[a] Soham Chowdhury,[a] Prakrati Patidar,[a] Depanjan Sarkar*,[ab] and Thalappil Pradeep*[abc]

[a] DST Unit of Nanoscience (DST UNS) & Thematic Unit of Excellence (TUE), Department of Chemistry
Indian Institute of Technology Madras (IITM)
Chennai 600036, India.

[b] Centre of Excellence on Molecular Materials and Functions, Department of Chemistry
Indian Institute of Technology Madras (IITM)
Chennai 600036, India.

[c] International Centre for Clean Water
2nd Floor, B-Block, IIT Madras Research Park, Kanagam Road
Taramani, Chennai 600113, India.
E-mail: depanjan_coe@icsrpis.iitm.ac.in, pradeep@iitm.ac.in

Table of contents

Serial No.	Description	Page No.
1	Experimental section	S3
2	Heavy Metal Adsorption Experiments	S3-S5
3	Characterization	S5-S6
6	Optical image of the reaction setup	S7
7	FESEM image of intermediate	S8
8	FESEM image of intermediate in a 1:1 and 2:1 ethanol-water mixture	S9
9	PXRD pattern of intermediate	S10
10	XPS plot of intermediate	S11
11	XPS survey spectrum of the final material	S12
12	PXRD pattern of silver oxide	S13
13	PXRD pattern of zinc-intermediate (zinc hydroxy acetate hydrate)	S14
14	TGA curve for intermediate and final material	S15
15	Optical image of intermediate in water after ultrasonic nebulization	S16
16	Optical image of intermediate in an ethanol-water mixture (4:1) after ultrasonic nebulization	S17
17	FESEM image of intermediate obtained via sonication	S18
18	Optical image of the as-synthesized tenorite (CuO) powder placed on an analytical balance	S19
19	BET surface area and pore structure analysis of the synthesized CuO nanostructures	S20
20	Linearized Langmuir isotherm	S21
21	Reusability of the hierarchical CuO adsorbent over nine cycles	S22
22	FESEM image of the nanostructured tenorite after U(VI) adsorption	S23
23	PXRD pattern of CuO after U(VI) adsorption	S24
24	XPS spectra of CuO after U(VI) adsorption	S25
25	References	S26

S1. Experimental section

Materials

Copper(II) acetate monohydrate ($[(CH_3COO)_2Cu \cdot H_2O]$, ≥98%) was purchased from Merck Specialities, India. Absolute ethanol (CH_3CH_2OH) AR was purchased from Zenith Trading Company, India. Methanol (CH_3OH) HPLC grade was purchased from Advent Chembio Pvt. Ltd, India. Uranyl nitrate hexahydrate $[UO_2(NO_3)_2.6H_2O]$ AR was purchased from Research-Lab Fine Chem Industries, India. Cupric oxide (CuO) powder was purchased from Sigma Chemical Company, USA. Ultrapure water (resistivity > 18.2 MΩ·cm) was used for all aqueous solution preparations. All the chemicals are commercially available and used as such without any purification.

Preparation of precursor solutions

A 0.04 M copper acetate monohydrate solution was prepared by dissolving 159 mg of copper acetate monohydrate in a solvent mixture of 16 mL of ethanol and 4 mL of Milli-Q water, followed by thorough sonication to ensure complete dissolution and obtain a homogeneous solution.

Reaction setup and experimental details

The copper acetate monohydrate precursor solution (Ethanol/Milli-Q water mixture) was transferred into a round-bottom flask and positioned on a water-bath assembly equipped with a 1.7 MHz ultrasonic nebulizer connected to a power supply. Continuous ultrasonic nebulization for 6 hours generated aerosolized microdroplets within the reaction chamber, promoting rapid solvent evaporation and intensified gas-liquid interfacial processes that drove precursor transformation. Following nebulization, the formed mist was allowed to settle, and the resulting precipitate was isolated by centrifugation (10,000 rpm, 5 min), washed, and air-dried. The dried intermediate was again renebulized in water for 3 hours to obtain a black suspension. The black suspension obtained was washed with water and an ethanol-water mixture, then centrifuged and air-dried to yield a blackish-brown precipitate.

S2. Heavy Metal Adsorption Experiments

For adsorption screening, 50 mg of the final product was added to 100 mL of aqueous solution, individually spiked with 1000 ppb of As(III), As(V), Se(IV), U(VI), Pb(II), and Cd(II) in separate

conical flasks. The suspensions were agitated on an orbital shaker for 3 hours to ensure sufficient interaction between the adsorbent and metal ions. After equilibration, the samples were centrifuged and filtered through nylon membrane filters. The metal ion concentrations in the initial (input) and treated (output) solutions were quantified using inductively coupled plasma mass spectrometry (ICP-MS).

Dosage-Dependent Adsorption Studies

To evaluate the effect of adsorbent dosage, varying amounts of the final material (5, 10, 20, 30, 50, 70, and 100 mg) were dispersed in separate conical flasks containing 100 mL of 1000 ppb U(VI) solution. The mixtures were shaken for 3 hours under identical conditions. Following agitation, each suspension was centrifuged, filtered, and analyzed by ICP-MS to determine the uranium concentration before and after treatment.

Adsorption Kinetics

Kinetic experiments were conducted by adding 20 mg of the material to a 100 mL solution containing 1000 ppb U(VI). The suspension was continuously shaken, and aliquots were collected at predetermined time intervals (0, 5, 10, 20, 30, 60, 90, and 120 min). Each aliquot was immediately centrifuged and filtered before ICP-MS analysis to monitor the time-dependent removal of U^{6+}.

Equation 1: Uptake capacity calculations

The adsorption capacity (q_e) of CuO for U(VI) was calculated using the following equation

$$\text{Uptake } (q_e) = (Co\text{-}Ce\ )V/m$$

where qe is the amount of U(VI) ions adsorbed per gram of adsorbent (mg/g) at equilibrium concentration, C_e is the equilibrium concentration of U(VI) in the bulk solution (mg/L), C_o is the initial U(VI) concentration (mg/L), V is the volume of solution (L) and m is the mass of adsorbent (g).

Equation 2: Rate constant calculations

Ho's pseudo-second-order equation is described as

$$t/q_e = 1/(k_2\, q_e^2) + (1/q_e)\, t$$

where q_e is the amount of U(VI) ions adsorbed per gram of adsorbent (mg/g), k_2 (g/mg min) is the pseudo-second-order rate constant.

From Fig. 5C, $1/q_e = 0.2147$ g/mg

Therefore, $q_e = 4.67$ mg/g

Also, $1/(k_2\, q_e^2) = 0.00378$ min g/mg

Therefore, $k_2 = 12.12$ g/mg min

Species	Model	k (g/mg min)	q_e (mg/g)	R^2
U (VI)	Pseudo 2nd order	12.12	4.67	1

Equation 3: Langmuir isotherm model

To investigate the maximum adsorption capacity, a series of U(VI) solutions with initial concentrations ranging from 1 to 100 mg/L(ppm) were shaken with the synthesized 20 mg CuO for 6 h at neutral pH. To account for the effect of equilibrium concentration on adsorption capacity, the Langmuir isotherm model was used for evaluation.

The linear form of the Langmuir equation is used

$$C_e/q_e = C_e/q_{max} + 1/(b\ q_{max})$$

where q_e is the amount of U(VI) ions adsorbed per gram of adsorbent (mg/g), C_e is the equilibrium concentration of U(VI) in the bulk solution (mg/L), q_{max} is the maximum surface density at monolayer coverage, and b is the Langmuir adsorption constant (L/mg) related to the free energy of adsorption.

From Fig. S15, $1/q_{max} = 0.00882$ g/mg

Therefore, $q_{max} = 113.37$ mg/g

Hence, $b = 0.27$ L/mg

S3. Characterization

To image the morphology of the intermediate and final product, a Thermo Fisher Scientific Verios G4 UC high-resolution field-emission scanning electron microscope (FESEM) was used at an accelerating voltage of 10 kV and an emission current of 0.10 nA. A thin layer of gold (~0.2 nm) was sputtered onto the sample and spread onto a carbon tape substrate using a Quorum Q150T S plus to make it conductive and suitable for FESEM imaging. To evaluate the crystallinity and elemental composition of the final product, the sample was drop-cast onto carbon-coated nickel TEM grids (300 mesh). Transmission electron microscopy (TEM) analysis was performed using a Thermo Fisher Scientific Talos™ F200i microscope operated at 200 kV. High-angle annular dark-field scanning transmission electron microscopy (HAADF-STEM) imaging, coupled with energy-dispersive X-ray spectroscopy (EDS), was employed to obtain elemental mapping of the particles. Lattice fringes in HRTEM images were measured using Gatan Microscopy software. Infrared spectra were recorded in attenuated total reflectance (ATR) mode using a PerkinElmer IR instrument within the range of 400-4000 cm^{-1}. XPS was performed using an ESCA probe TPD spectrometer (Omicron) with a polychromatic Al kα (hv = 1486.6 eV) X-ray source to determine the chemical oxidation states of the elements. Powder XRD measurements were performed by using a D8 Advance Bruker instrument, using Cu Kα as the X-ray source. Quantitative

determination of uranium and other metal concentrations was conducted using a PerkinElmer NexION 300X ICP-MS calibrated with appropriate reference standards. Brunauer-Emmett-Teller (BET) measurements were performed on approximately 50 mg of the material using a Micromeritics ASAP 2020 Porosimeter to determine surface area. Thermogravimetric analysis (TGA) was conducted on a Q500 Hi-Res Thermogravimetric analyzer using approximately 10 mg of material.

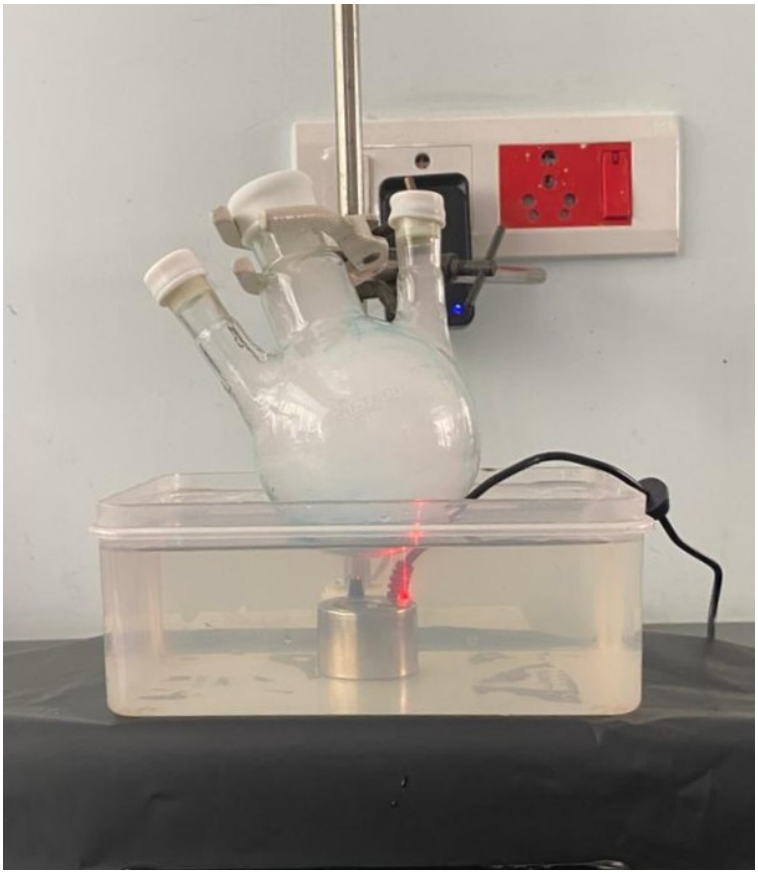

Fig. S1. Optical image of the experimental setup used for ultrasonic nebulization during the reaction.

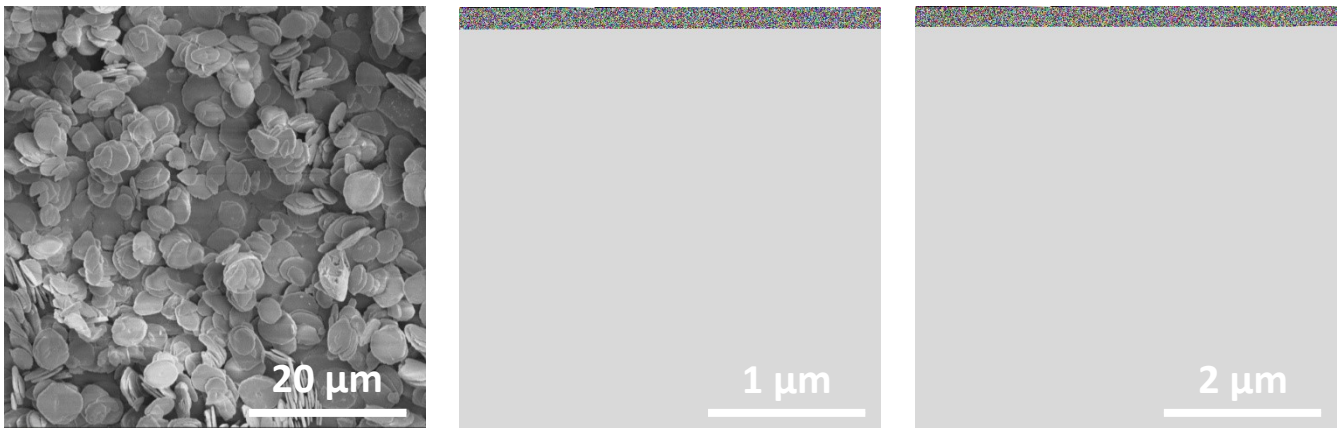

Fig. S2. FESEM images of copper hydroxide acetate monohydrate (intermediate).

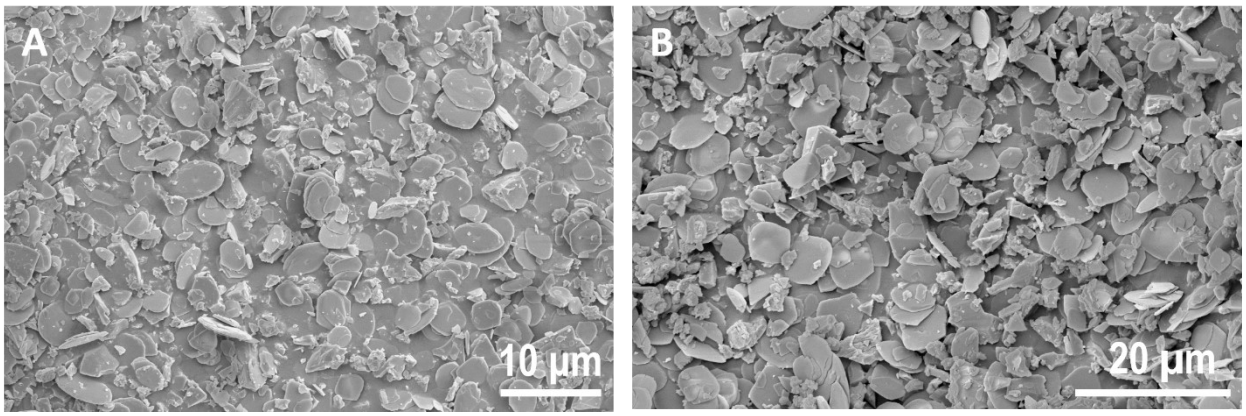

Fig. S3. FESEM images of intermediate. (A) Ethanol-water mixture of 1:1 ratio and (B) Ethanol-water mixture of 2:1 ratio.

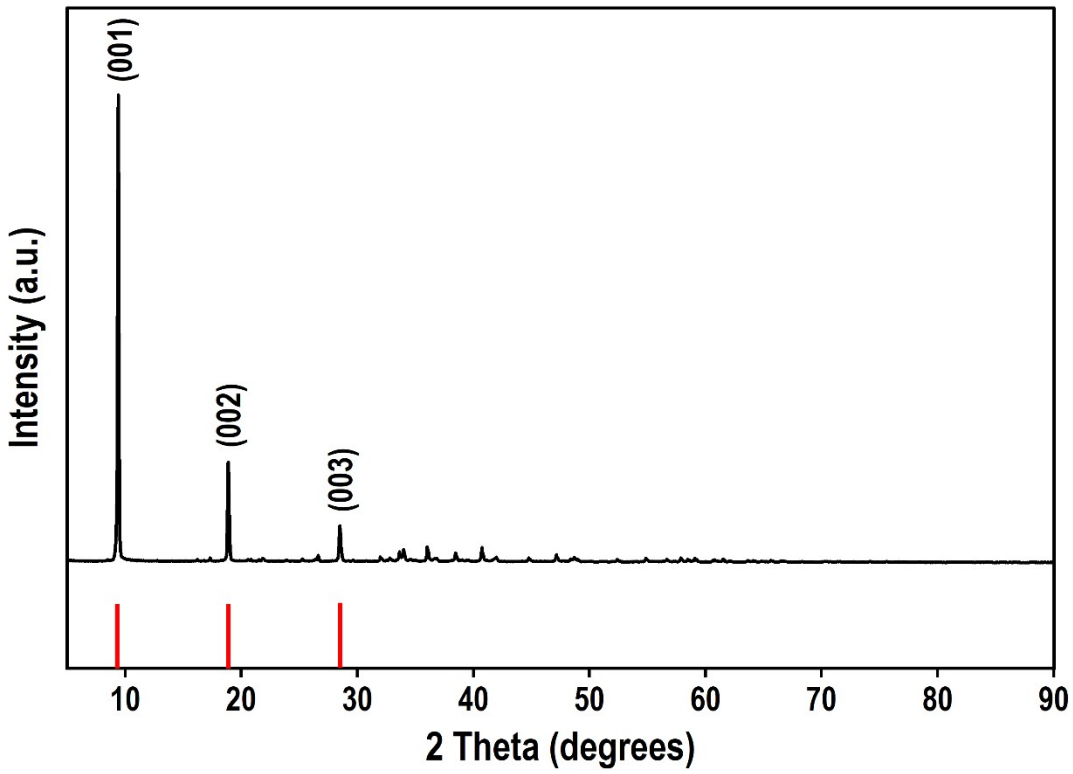

Fig. S4. PXRD pattern of intermediate.[1]

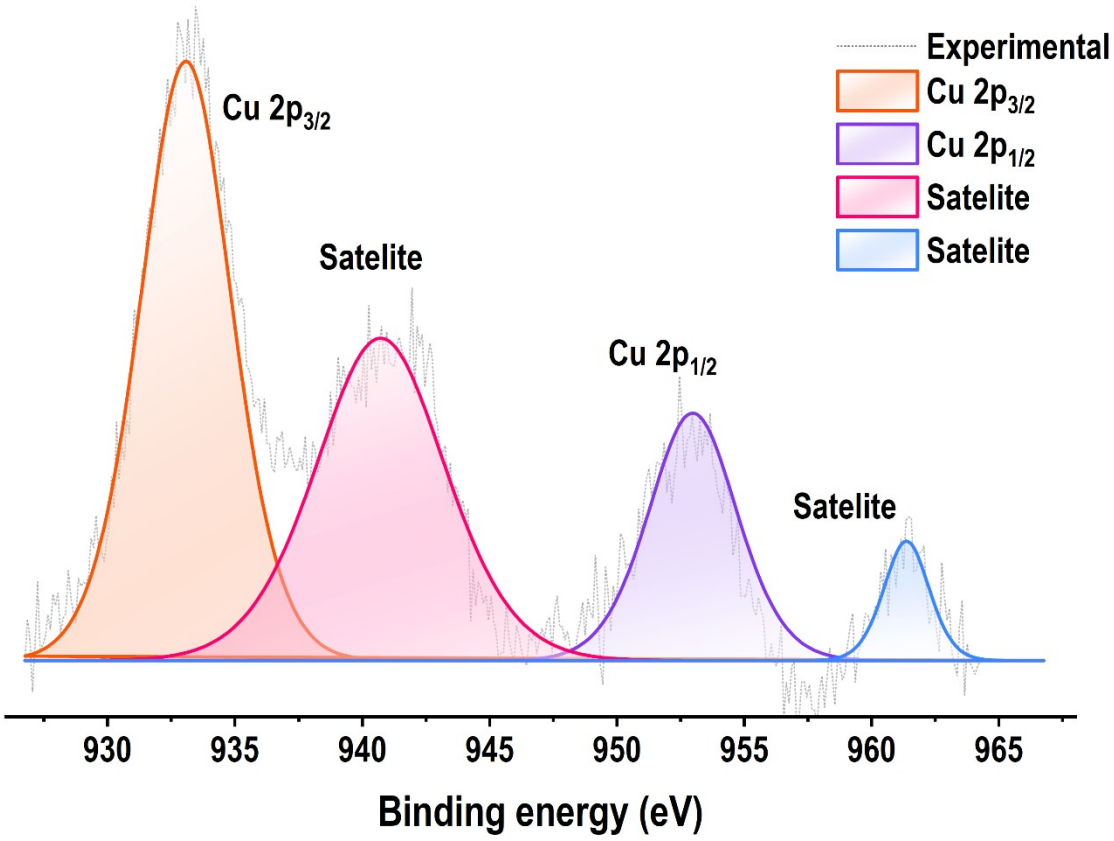

Fig. S5. XPS plot of intermediate.

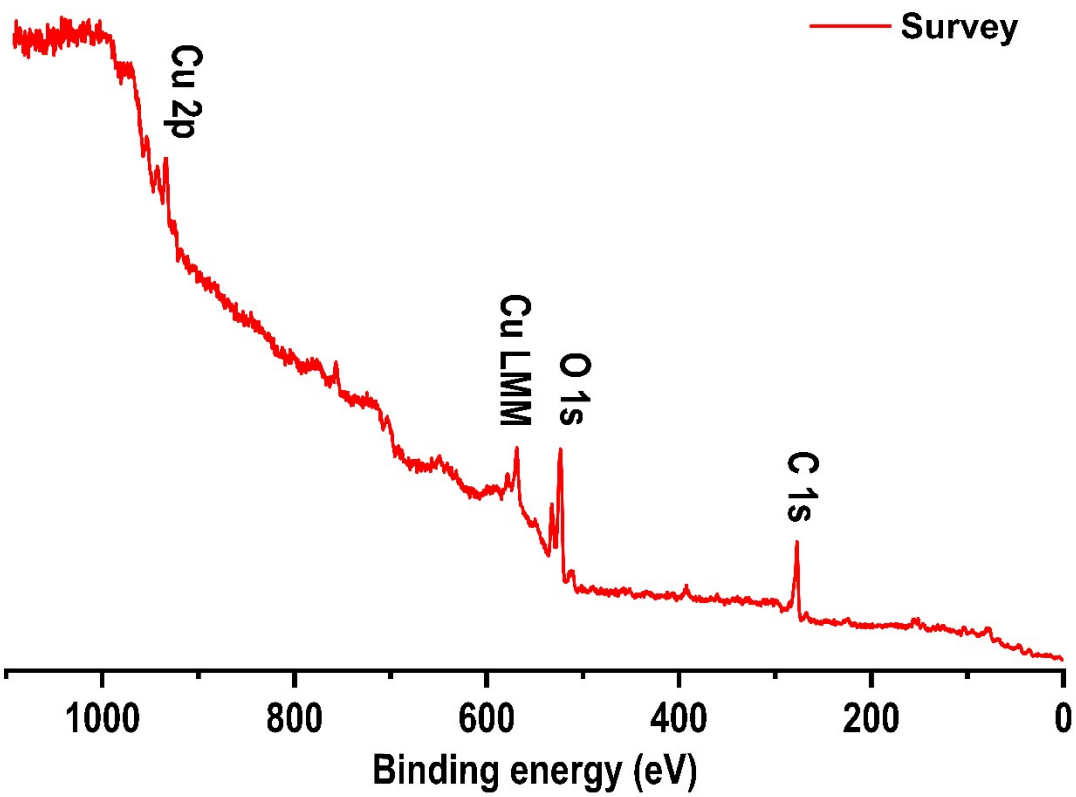

Fig. S6. XPS survey spectrum of the final material, verifying the presence of Cu and O elements, (C is due to the carbon tape used for support).

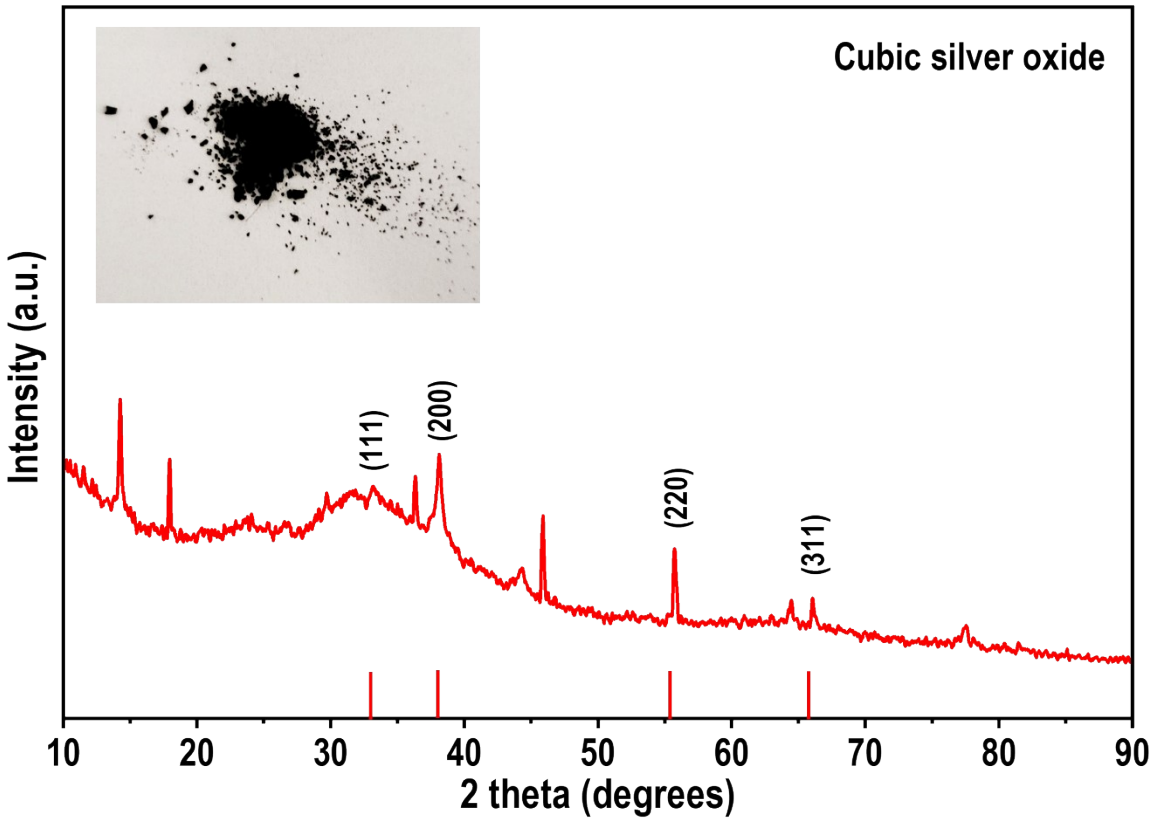

Fig. S7. PXRD pattern of silver oxide, the inset shows the optical image of the precipitate obtained after reaction.

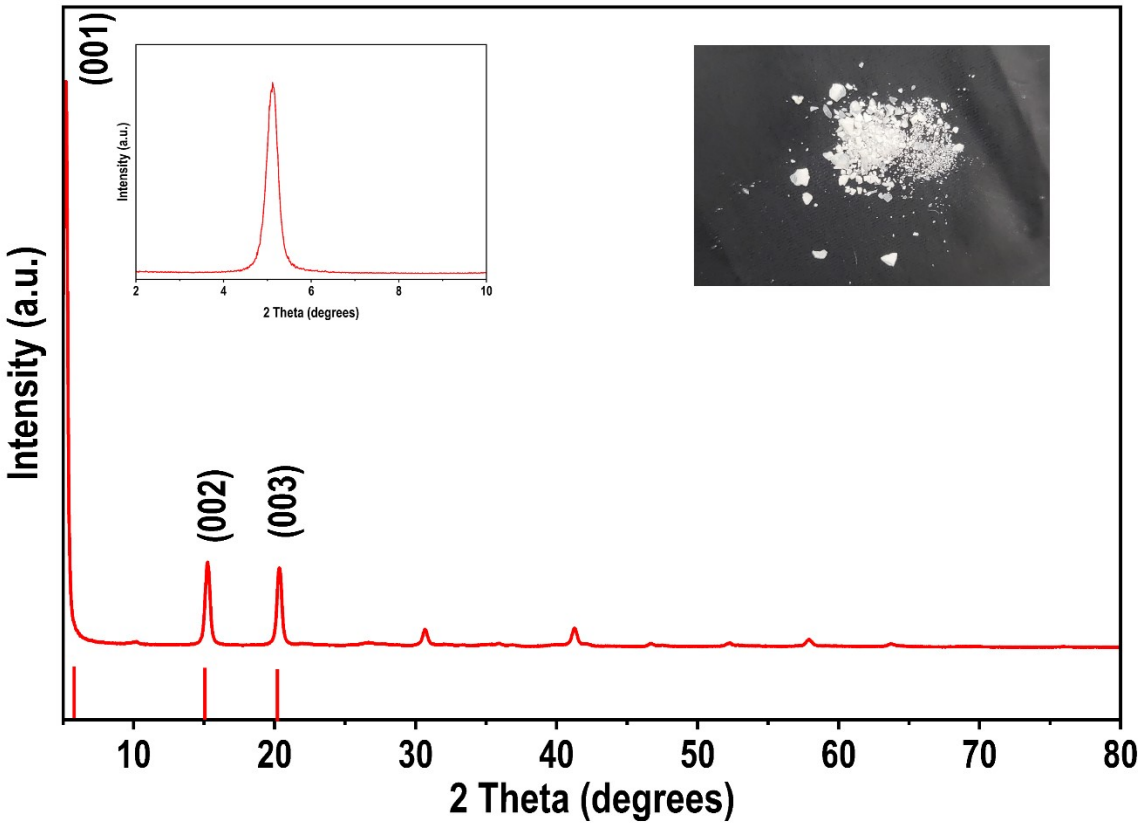

Fig. S8. PXRD pattern of zinc-intermediate (zinc hydroxy acetate hydrate), the inset shows the optical image of the precipitate obtained after reaction.

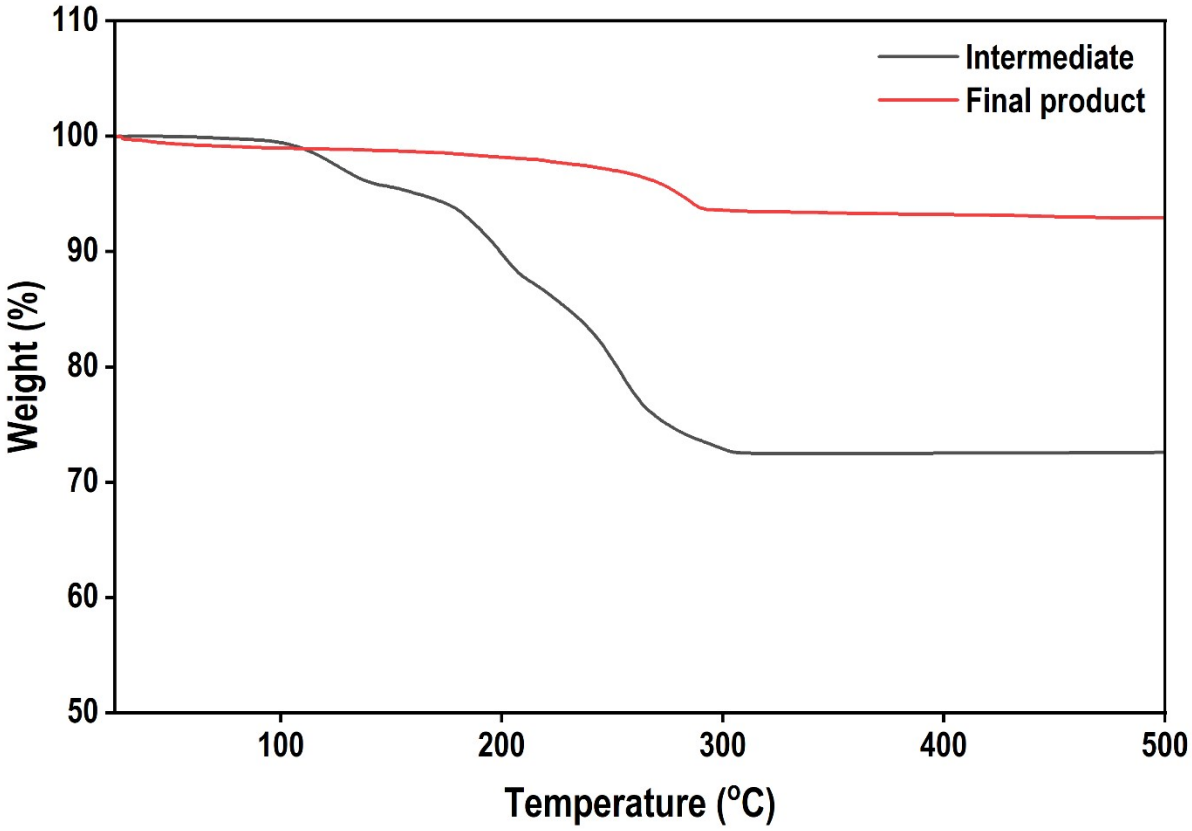

Fig. S9. TGA curve for intermediate and final product (tenorite).

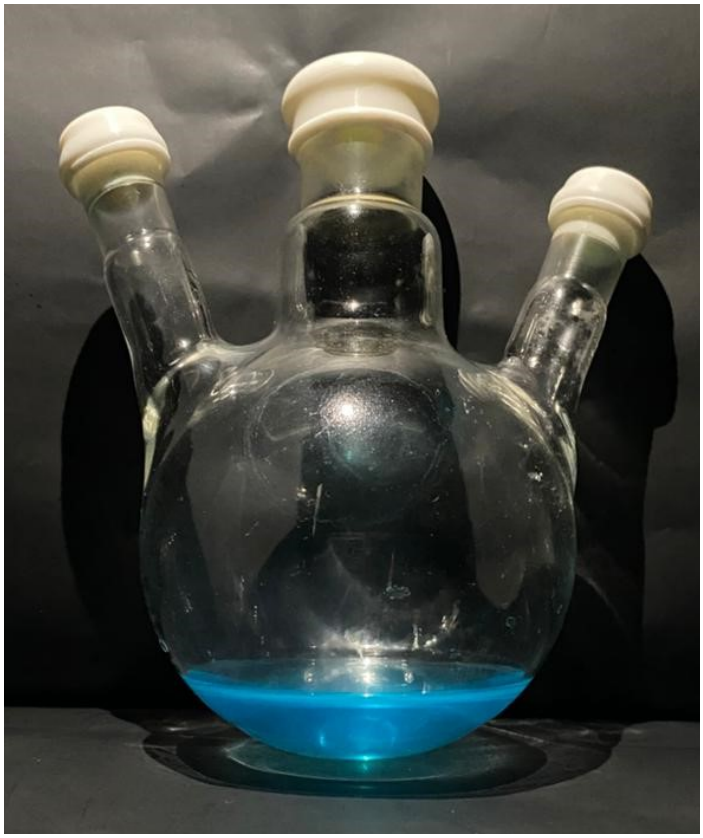

Fig. S10. Optical image of precursor solution in water after ultrasonic nebulization, showing no precipitate.

Fig. S11. Optical image of the precipitate after ultrasonic nebulization of the precursor solution in an ethanol-water mixture (4:1).

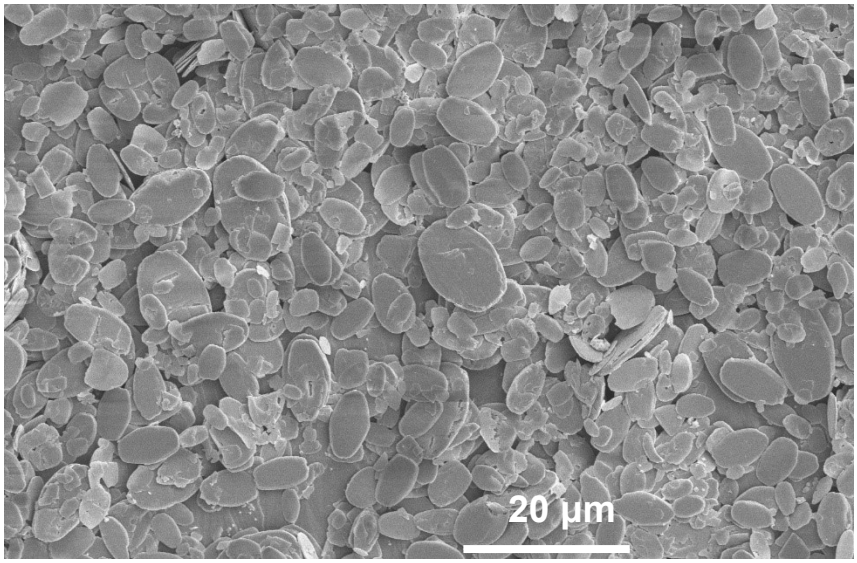

Fig. S12. FESEM of intermediate obtained via sonication of the precursor in EtOH: H_2O (4:1).

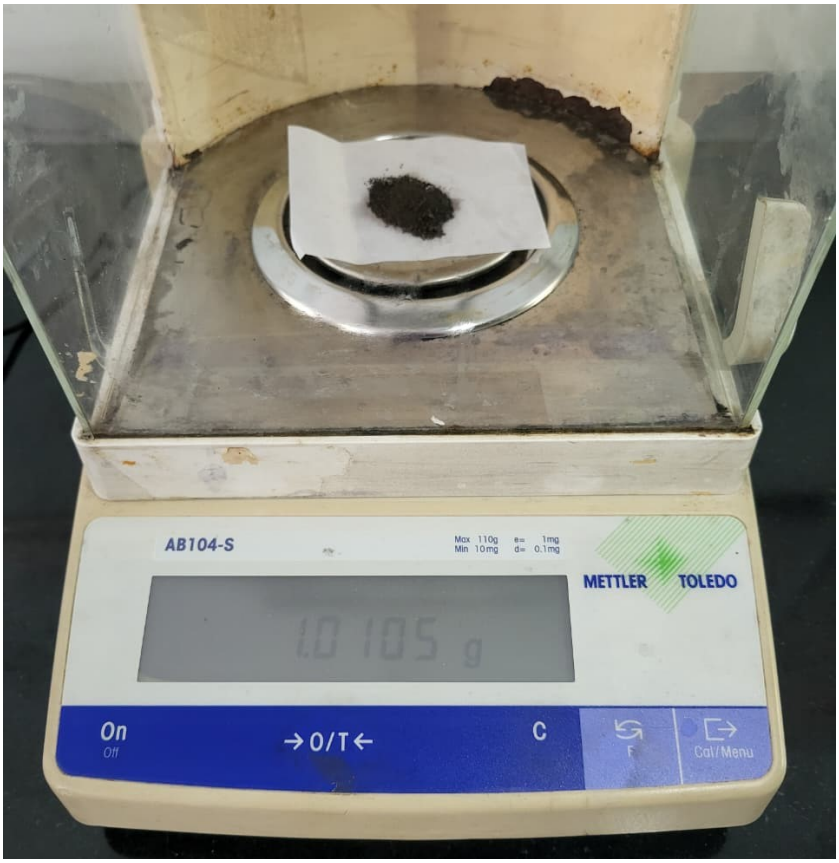

Fig. S13. Optical image of the as-synthesized tenorite (CuO) powder placed on an analytical balance demonstrating gram-scale synthesis.

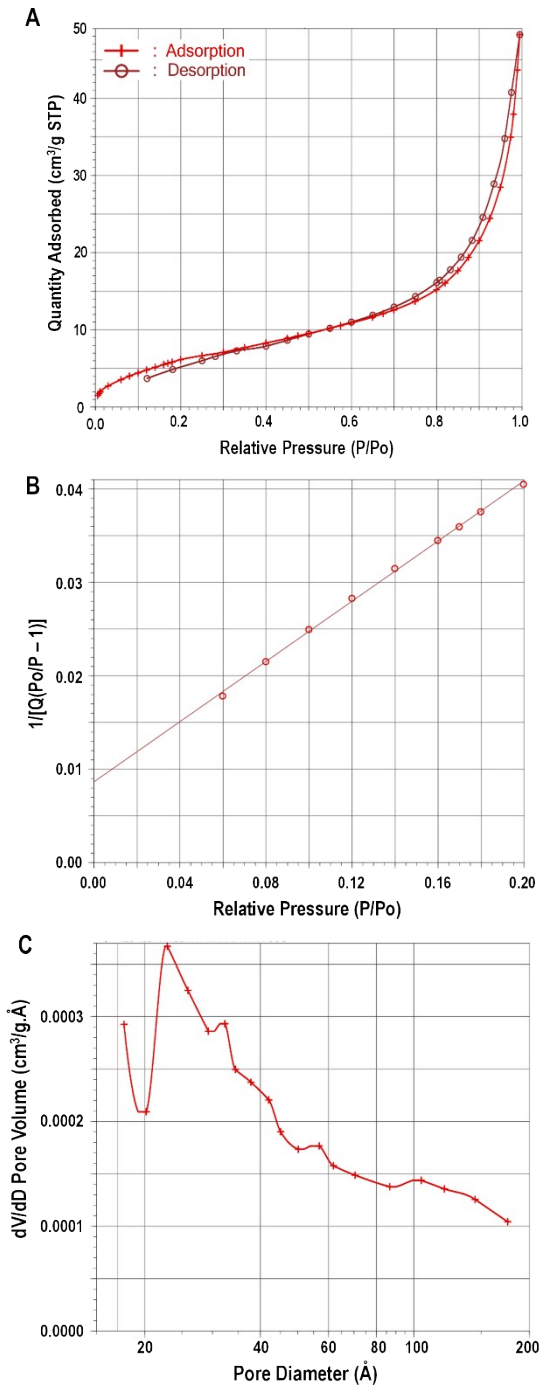

Fig. S14. Brunauer-Emmett-Teller (BET) surface area and pore structure analysis of the synthesized tenorite nanostructures. (A) N_2 adsorption-desorption isotherms showing mesoporous characteristics. (B) BET linear plot used for specific surface area determination. (C) The Barrett-Joyner-Halenda (BJH) pore-size distribution curve indicates the presence of mesopores arising from the hierarchical architecture. BET Surface Area: 25.6281 m^2/g.

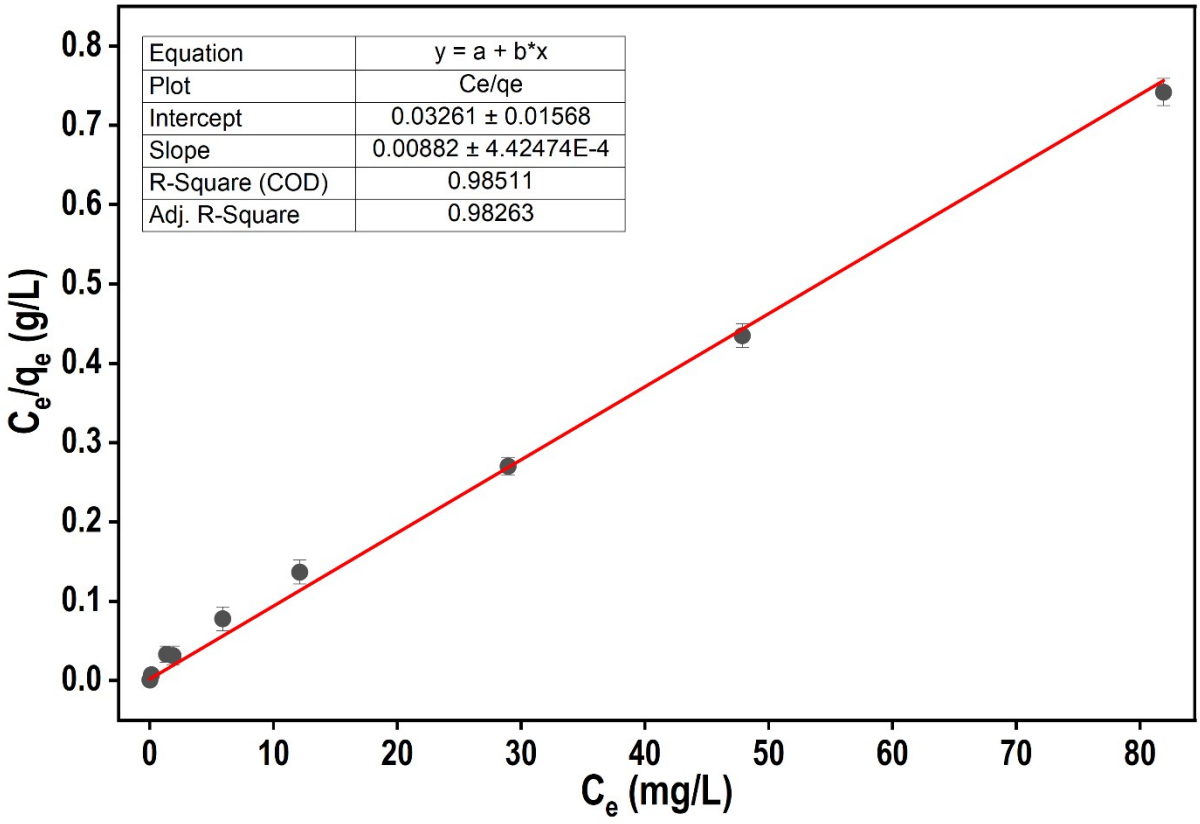

Fig. S15. Linearized Langmuir isotherm for the adsorption of U(VI) on synthesized CuO (C_e/q_e vs C_e).

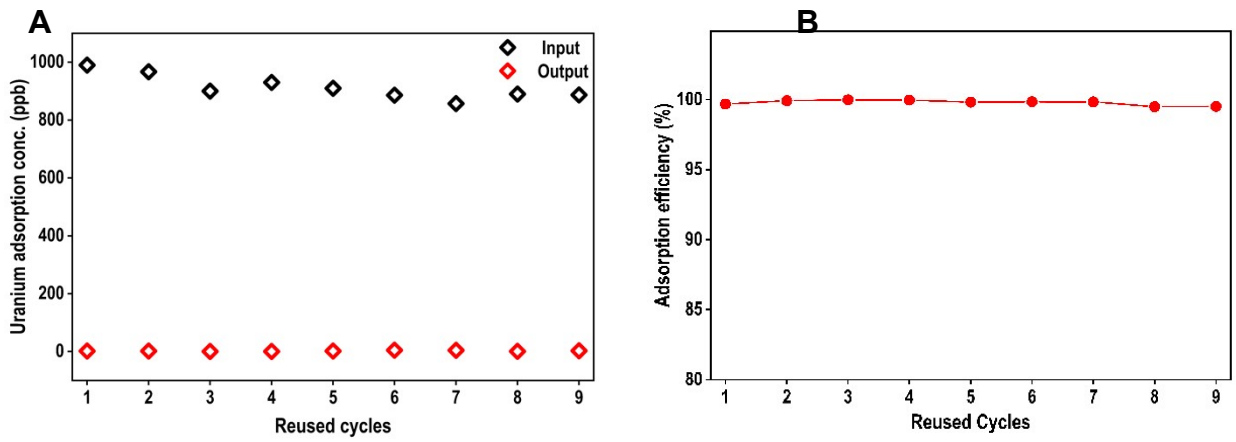

Fig. S16. Reusability of the hierarchical CuO adsorbent for U(VI) removal over nine consecutive cycles. (A) Input and output U(VI) concentrations during repeated adsorption experiments. (B) Corresponding adsorption efficiency, showing negligible loss in performance upon reuse.

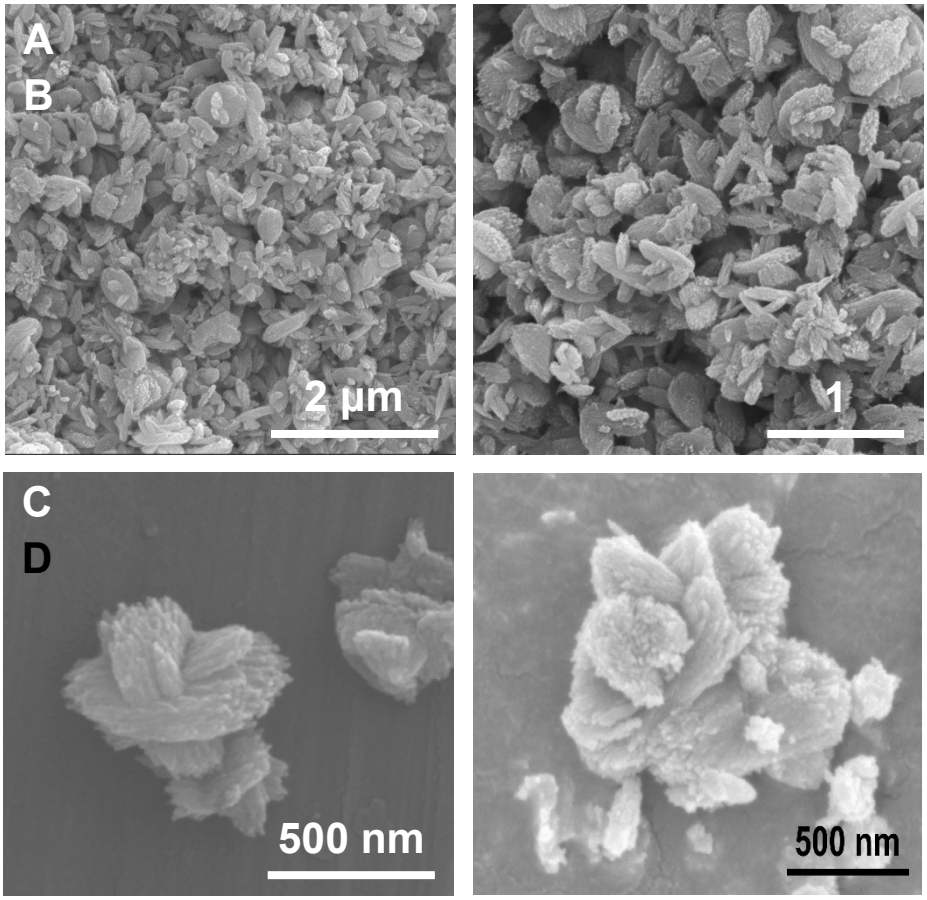

Fig. S17. FESEM image of the nanostructured tenorite after U(VI) adsorption. (A, B, C) After a single adsorption cycle and (D) after 9 adsorption cycles.

.

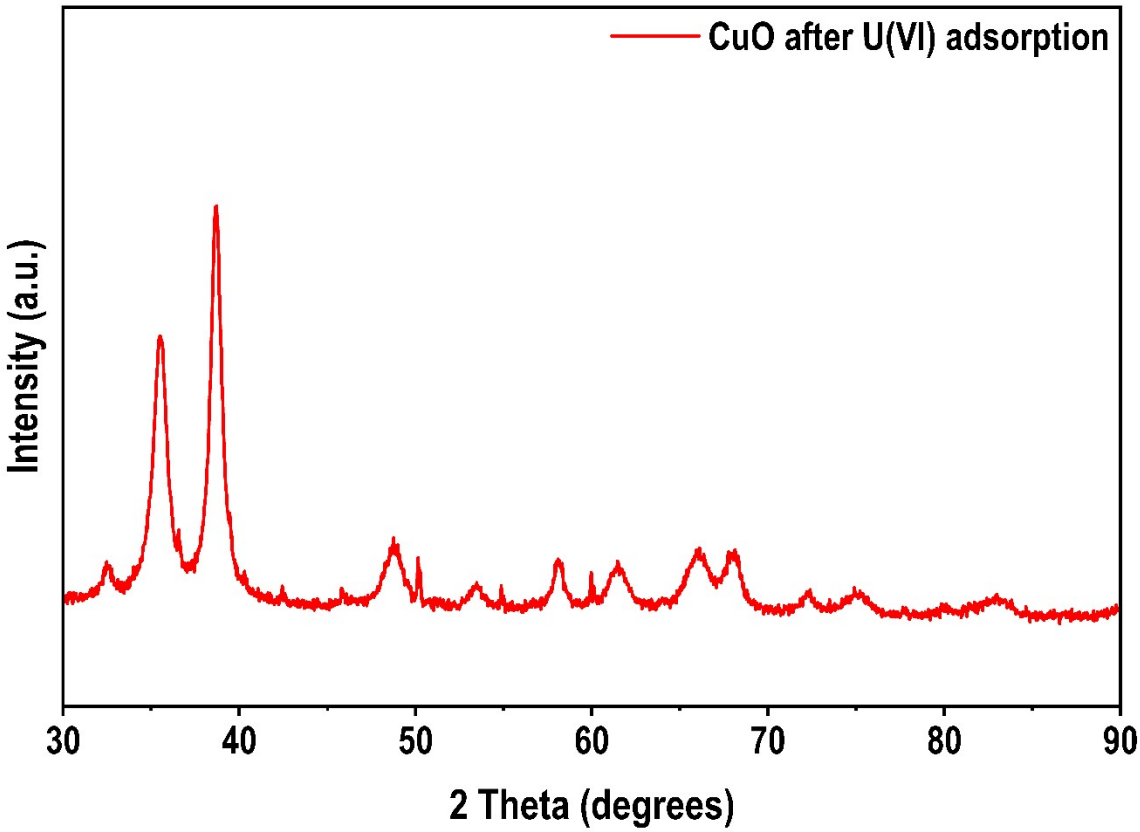

Fig. S18. PXRD pattern of CuO after U(VI) adsorption, showing no significant changes in the diffraction features and indicating preservation of the crystal structure following adsorption.

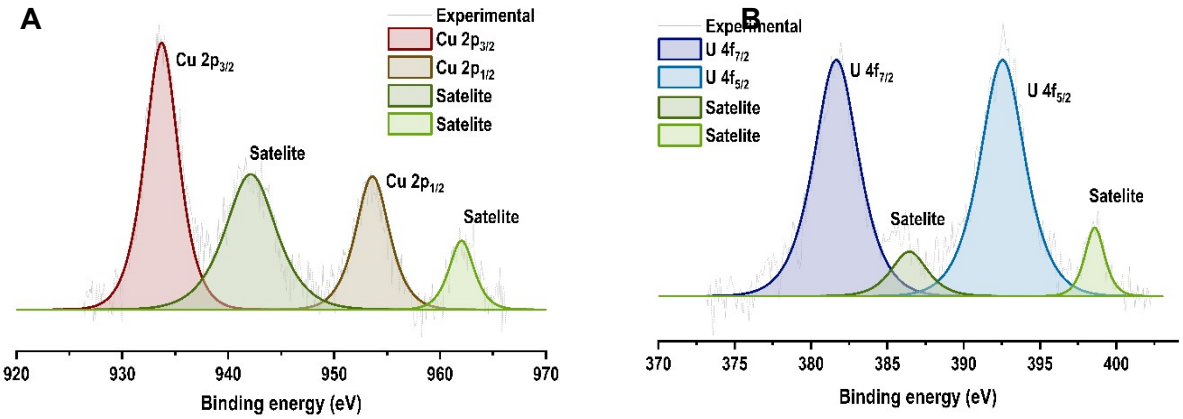

Fig. S19. XPS spectra of the CuO after U(VI) adsorption. (A) Cu 2p and (B) U 4f regions, confirming the presence of adsorbed uranium species on the CuO surface.

Reference

1 S. Švarcová, M. Klementová, P. Bezdička, W. Łasocha, M. Dušek and D. Hradil, *Cryst. Res. Technol.*, 2011, **46**, 1051–1057.